Microrheology of the Liquid-Solid Transition during Gelation

Travis H. Larsen and Eric M. Furst*

Department of Chemical Engineering and Center for Molecular and Engineering Thermodynamics, University of Delaware, Newark, Delaware 19716, USA

(Received 3 January 2008; published 11 April 2008)

The viscoelastic properties of physical and chemical polymer gels are characterized through the liquid-solid transition using particle tracking microrheology. Measurements of the probe particle mean-squared displacement are shifted as the extent of gelation increases to generate master curves. From the shift factors, we determine the gel point and critical scaling exponents. Both systems exhibit a critical relaxation exponent $n \approx 0.6$, where $G' \sim G'' \sim \omega^n$ for the incipient gel, consistent with the Rouse model of dynamic scaling in the percolation universality class.

DOI: 10.1103/PhysRevLett.100.146001 PACS numbers: 83.85.Cg, 64.60.F−, 81.16.Fg, 83.80.Kn

The gelation of both naturally occurring and engineered biomaterials have been increasingly characterized using microrheology, in which the thermal motion of dispersed microspheres is used to probe changes in rheology throughout the liquid-solid (sol-gel) transition [1–6]. Advantages of microrheology include exquisite sensitivity that enables the characterization of weak, incipient polymer networks, the ability to capture systems with rapid gelation kinetics that pass quickly through the liquid-solid transition, and access to materials for which only small quantities are available. However, while methods for determining the gel point and other physical characteristics of the liquid-solid transition have been well described for bulk rheological measurements, robust methods for determining these from microrheology experiments have not been reported, despite the growing importance of microrheology for characterizing emerging and scarce materials.

The liquid-solid transition for polymeric gels has been a subject of intense study due to its fundamental and engineering significance. Because of the nature of the percolation transition at the gel point, gelling materials exhibit critical behavior, which is manifested by the divergence of several physical properties, including the zero shear viscosity, equilibrium modulus and longest relaxation time [7,8]. Perhaps most intriguing, however, is the fact that the viscoelastic moduli of the critical gel exhibit frequency independent power-law scalings, $G' \sim G'' \sim \omega^n$, where n is the critical relaxation exponent [9]. The relaxation exponent has proven not to have a constant value, but rather varies with the characteristics of the network connectivity [10]. This complicates the interpretation of gelation data using microrheology when n is not known *a priori* [4], and many studies assume $n = 0.5$, corresponding to $G' = G''$. Overall, it is critical to define both the gel point and the scaling exponent, since these provide unique insight into the kinetics, rheology, and microstructure of a gelling material.

Here, we present a study of the liquid-solid transitions of both physically cross-linked biomaterial gels and chemically cross-linked polymeric gels. Using the scaling principles of time-cure superposition [11], we identify the gel point, critical relaxation exponent and dynamic scaling exponents from tracer particle dynamics measured using multiple particle tracking microrheology. This demonstrates that microrheology can be used to extract the entire spectrum of rheological characteristics at the gelation transition, similar to macrorheology.

The first experimental system is a 20-residue peptide that, when triggered by changes in the solution pH or ionic strength, folds into an amphiphillic β-hairpin. The folded peptide molecules subsequently self-assemble with time to form a network of physically cross-linked semiflexible filaments [12,13]. The peptide used here is a derivative of a previously described parent peptide (MAX1), which consists of an alternating sequence of valine and lysine residues surrounding a tetrapeptide sequence with a high β-turn propensity [12,14]. Such self-assembling oligopeptides are representative of many new and emerging biomaterials, whose mechanical and biofunctional properties can be tailored through the rational design of an amino acid sequence.

We demonstrate the generality of the liquid-solid transition microrheology by comparing results obtained using chemically cross-linked polyacrylamide gels, in which the polymer cross-linking is controlled by the concentration of bis-acrylamide. Thus, while the peptide hydrogels represent a dynamic, physically gelling system that is dependent on self-assembly time, the polyacrylamide gels are equilibrated and stationary systems in which the extent of gelation is controlled by the amount of added cross-linker.

Sample preparation.—Peptide is synthesized using a solid-phase Fmoc synthesis, purified by reverse phase HPLC, and then lyophilized for storage. Further details have been reported previously [12]. Peptide stock solutions are prepared by redispersing lyophilized peptide with gentle agitation in water (conductivity 18.2 $M\Omega \cdot cm$) immediately before each experiment. The gelation process is initiated by increasing the pH with the addition of buffer. The final sample contains 0.15 wt % peptide in pH 8.5 buffer (50 mM BTP).

Polyacrylamide monomer, bis-acrylamide cross-linker, TEMED catalyst, and ammonium persulfate initiator are obtained commercially (Sigma Aldrich). Stock solutions are made daily and degassed prior to use. Samples are prepared at 3.0 wt % total acrylamide, including up to 0.1 wt % bis-acrylamide, 0.5 wt % ammonium persulfate, and 0.1% TEMED.

Fluorescent polystyrene microspheres with diameter $2a = 1.05 \pm 0.01$ μm, (Polysciences, Warrington, PA) serve as tracer particles in both systems. Particles are washed 3 times with ultrapure water and sonicated prior to use. They are added to a final concentration of 0.15 v % before gelation is initiated.

Multiple particle tracking microrheology.—Rectangular capillary cells ($0.20 \times 2.00 \times 50$ mm, Vitrotubes, Vitrocom) are used as sample chambers to eliminate convection due to leakage or evaporation. After gelation is initiated for either system, the solution is introduced by capillary action, the vial ends are cut to remove excess air and sealed with fast-curing UV epoxy (Norland Products, NOA 81) to a microscope slide. Data collection begins immediately for the peptide solutions, while the polyacrylamide samples are allowed to equilibrate for 6 h before measurements are performed. In the latter, ultraviolet-visible spectroscopy is used to monitor the polymerization reaction (data not shown), to ensure that this is sufficient time to reach an equilibrated state.

The embedded fluorescent microspheres are imaged at a total magnification of 63× using an inverted epifluorescence microscope (numerical aperture of 1.2, 63× water-immersion objective, 1.0× tube lens, Axiovert 200, Zeiss). The motion of roughly 150 in-frame particles is captured for a total of 800 frames at 30 Hz with a CMOS high-speed camera (Phantom v5.1, Vision Research). A large number of viewable particles and short burst times ensure adequate tracking statistics while capturing quasistationary gelation states. Particle tracking is performed using a weighted centroid method, and the ensemble-averaged mean-squared displacement, $\langle \Delta r^2(\tau) \rangle$, is calculated [15]. We note that the high-magnification immersion objective and short exposure time ($\sigma = 1000$ μs) are necessary to reduce the static and dynamic contributions to error in the particle trajectory analysis [16].

Mean-squared displacement (MSD).—The calculated mean-squared displacements are plotted versus lag time in Fig. 1. Individual curves represent measurements taken at different points in the gelation process. For the peptide, data is collected continuously, thus each curve is a measurement at increasing time points after the self-assembly process is initiated. For polyacrylamide samples, each MSD curve represents a separate sample prepared with increasing cross-linker concentration. At short times and low cross-linker concentrations, the system exhibits a purely viscous response, characterized by a $\langle \Delta r^2(\tau) \rangle \sim \tau$. As time or cross-linker concentration increases, there is a continuous decrease in the magnitude of the mean-squared displacement, and emerging dependence on lag time. Subdiffusive behavior initially occurs at short lag times, and the MSD exhibits a crossover to diffusive behavior at longer lag times. At still longer times or higher cross-linker concentrations, the dynamics at long lag times also become subdiffusive, even exhibiting a distinct plateau in the polyacrylamide case, consistent with the formation of a viscoelastic solid. After this point, the MSD across all lag times decreases further, and approaches a constant value, as expected for an elastic solid with modulus G_0, where $\langle \Delta r^2(\tau) \rangle = k_B T / \pi a G_0$.

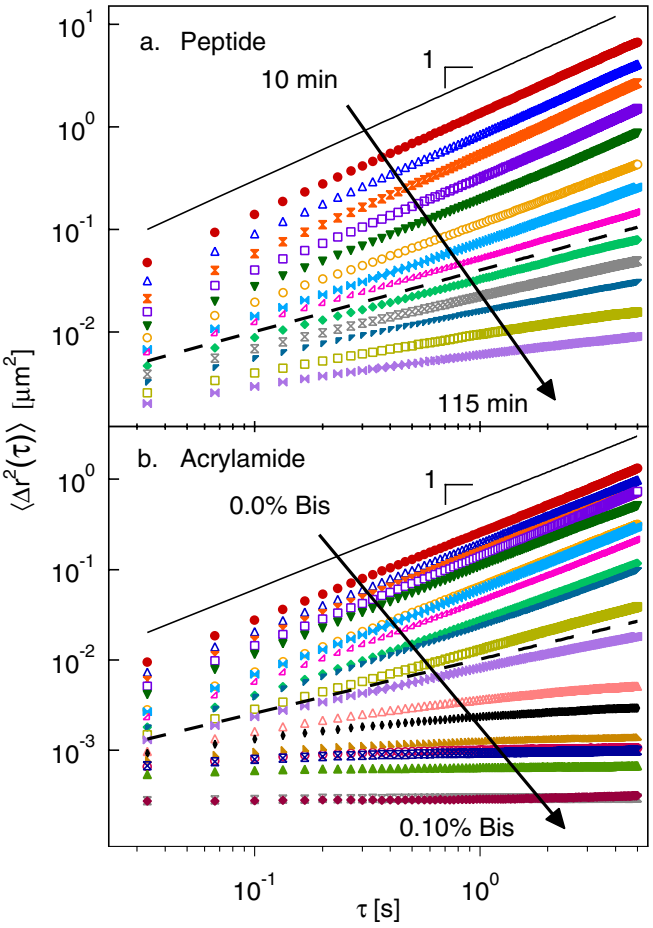

FIG. 1 (color online). Ensemble-averaged mean-squared displacement $\langle \Delta r^2(\tau) \rangle$ of embedded polystyrene microspheres ($2a = 1.05 \pm 0.01$ μm) plotted versus lag time. Individual curves represent the particle dynamics at various extents of gelation. (a) Self-assembly of a 0.15 wt % peptide solution is initiated by the addition of buffer, and gelation proceeds with time, t, from 10–115 min. (b) Gelation of equilibrated 3.0 wt % polyacrylamide gels with bis-acrylamide cross-linker concentrations from 0.0–0.10 wt %. Dashed lines indicate the gel point and have logarithmic slopes of 0.6 and 0.55 for the peptide and polyacrylamide systems, respectively.

The generalized Stokes-Einstein relation describes these tracer particle dynamics in terms of the viscoelastic properties of the gelling material, $\langle \Delta r^2(t) \rangle = \frac{k_B T}{\pi a} J(t)$, written

here in terms of the creep compliance $J(t)$, where a is the radius of the probe particles and k_BT is the thermal energy [17–19]. $J(t)$ relates the material strain deformation $\gamma(t)$ to the rate of applied stress $\dot{\sigma}(t)$ via $\gamma(t) = \int_0^t J(t-t')\dot{\sigma}(t)dt'$ [20]. The direct proportionality of the MSD and creep compliance avoids artifacts in converting the data to the more commonly used frequency-dependent moduli [19].

We can now use $J(t)$ to interpret the tracer dynamics shown in Fig. 1. Initially, the subdiffusive dynamics at short lag times is due to the relaxation of the Rouse-like fluctuations of the growing polymer clusters, while the diffusion of clusters dominates the dynamics and rheology at lag times beyond the longest relaxation time. As the polymer clusters grow in size in the pre-gel, the increase in the longest relaxation time τ_L is evident by the increase in time required for the MSD scaling to recover to unity. At the critical gel point, the percolating network forms an infinite, sample-spanning cluster, and τ_L diverges to infinity [8]. At this point, the MSD exhibits a power-law dependence over all times, since $J_c(t) = \frac{\sin n\pi}{n\pi S} t^n$, where S is the gel strength with units $\mathrm{Pa}\cdot\mathrm{s}^n$ and n is the critical relaxation exponent [9]. Beyond the gel point, continued growth of the network leads to increased entanglements and cross-links with a corresponding decrease in τ_L along with a plateau reflecting the equilibrium modulus.

Gel point and critical behavior.—Master curves are constructed by shifting individual MSD curves along the ordinate and abscissa. As shown in Fig. 2(a), starting from the initial diffusive dynamics, subsequent MSD curves are multiplied by a time-shift factor a and an MSD shift factor b. The resulting master curve has logarithmic slope $\alpha = d\ln\langle\Delta r^2(\tau)\rangle/d\ln\tau = 1$ at long scaled lag times $a\tau$, which decreases monotonically to a value between $0.55 \leq \alpha \leq 0.6$ with decreasing $a\tau$. At this point, subsequent curves can no longer be scaled onto this initial master curve. A second master curve is constructed, beginning with the MSD data collected at longest times or greatest cross-linker concentrations. In this case, the initial values of α at long $a\tau$ are between 0–0.25, reflecting a viscoelastic solid or onset of a long-time plateau. At short lag times, α converges to a value similar to that of the first master curve.

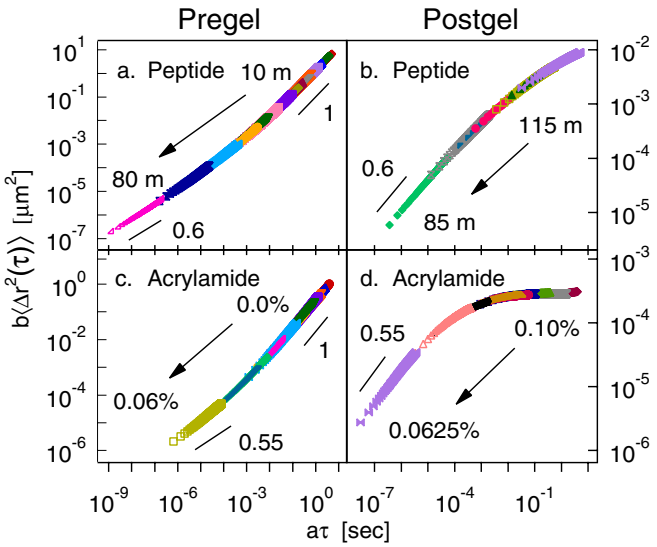

FIG. 2 (color online). Superposition of the MSD from Fig. 1. Master curves are created before and after the gel point for the peptide (a) and polyacrylamide (b) gels by shifting the data vertically, $b\langle\Delta r^2(\tau)\rangle$, and horizontally, $a\tau$, to account for changes in the MSD and longest relaxation time as the connectivity of the percolating network increases.

The resulting shift factors, a and b, plotted with respect to time t (peptide) or cross-linker concentration p (polyacrylamide), are shown in Fig. 3. Starting from the first pre-gel measurement, the shift factors decrease towards an asymptote as time or concentration increases. Likewise, the shift factors determined from the final MSD reference also exhibit an asymptote as the time or concentration decreases. The divergence of a and b is consistent with the critical behavior of the gelation transition, and thus identifies the incipient, or critical, gel. This behavior can be explained by relating the shift factors to the divergence of physical properties using scaling relationships derived from percolation theory [11]. In the vicinity of the gel point, the time-shift factor, a, reflects the divergence of the longest relaxation time τ_L [8,21]. Similarly, the MSD shift factor b captures the divergence of the steady-state creep compliance J_e^0. The gel points found using both shift factors are consistent, and marked by the dashed lines in Fig. 3. The gel point for 0.15 wt % peptide is $t_c = 82$ min, while the gel point for 3.0 wt % polyacrylamide is $p_c = 0.062$ wt % bis-acrylamide.

Identification of the gel point, which marks the transition from a liquid to a solid, enables us to define the distance from the critical gel point, $\varepsilon = |t - t_c|/t_c = |p - p_c|/p_c$. Near the gel point, the longest relaxation time and creep compliance are expected to exhibit power-law behavior, $\tau_L \sim \varepsilon^{-y}$ and $J_e^0 \sim \varepsilon^{-z}$ [11]. The dynamic scaling expo-

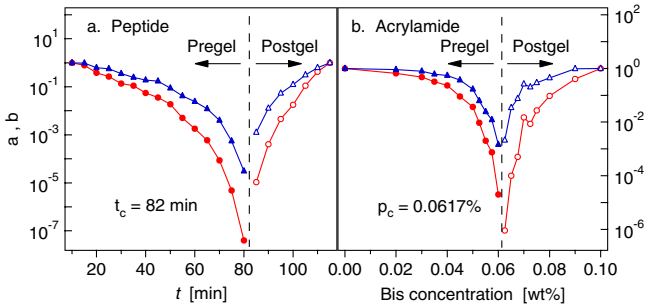

FIG. 3 (color online). Shift factors a (red circles) and b (blue triangles) used for superposition in Fig. 2 are plotted as a function of self-assembly time, t, for (a) the peptide hydrogel and (b) as a function of cross-linker concentration for the polyacrylamide gels. The critical gel point, t_c or p_c, is determined by the asymptotic behavior, illustrated by the dashed vertical line.

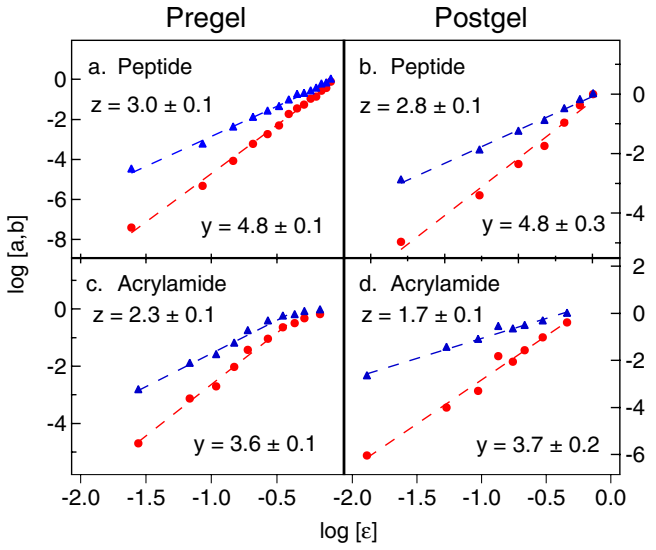

FIG. 4 (color online). Shift factors a (red circles) and b (blue triangles) are plotted versus the distance from the gel point, ε, for (a) peptide pregel, (b) peptide postgel, (c) polyacrylamide pregel, and (d) polyacrylamide postgel. Dashed lines are linear fits of the logarithmic data with the corresponding dynamic scaling exponents shown.

nents, y and z, are determined for both the pre- and postgels shown in Fig. 3. In both cases, the shift factors correspond to $a \sim \tau_L^{-1}$ and $b \sim 1/J_e^0$. As shown in Fig. 4, a and b exhibit the expected power-law behavior when plotted versus ε. For the peptide, the agreement between the scaling exponents on either side of the gel point is excellent, with $y = 4.8 \pm 0.2$ and $z = 2.9 \pm 0.1$. In the case of polyacrylamide, the scaling exponents are $y = 3.7 \pm 0.1$ and $z = 2.0 \pm 0.1$. For both systems, the values of the critical exponents are in reasonable agreement with those predicted using dynamic scaling based on a percolation universality class when hydrodynamic interactions are screened (Rouse theory). In this case, fractal gels composed of small-molecule precursors, similar to those employed here, are expected to exhibit the dynamic scaling exponents $y = 4$ and $z = 8/3$ [22]. In contrast, the exponents predicted from Zimm theory (unscreened hydrodynamic interactions) are $y = 8/3$ and $z = 8/3$ [22], and de Gennes' electrical network analogy leads to $y = 2.69$ and $z = 1.94$ [23].

Finally, the dynamic exponents are related to the critical relaxation exponent by $n = z/y$ [11]. For 0.15 wt % peptide and 3.0 wt % polyacrylamide, the scaling exponents for the critical gel are $n = 0.60 \pm 0.02$ and $n = 0.55 \pm 0.03$, respectively. Again, these values are consistent with Rouse dynamics, for which $n = 2/3$. Notably, the relaxation exponent determined from the critical scaling behavior is in excellent agreement with the slope of the MSD curves close to the gel transition point, as shown by the dashed lines in Fig. 1 and the slope of the MSD master curves in Fig. 2, confirming the power-law dependence of $J(t)$ at the gel point.

Conclusion.—Multiple particle tracking microrheology was successfully used to measure the critical gelation of both peptide and polyacrylamide solutions. Utilizing the connectivity-based scaling principles of time-cure superposition, the probe particle mean-squared displacements are collapsed onto master curves before and after the gel point. The gel point, critical relaxation exponent and dynamic scaling exponents were found from the lag time and MSD shift factors. The critical exponents determined for both systems compared well with those reported for Rouse dynamics of fractal polymers. Most importantly, the analysis we present offers a means for characterizing the gelation process of weak or fast-forming gels that could previously not be measured using traditional bulk rheological techniques.

We thank J. Schneider and K. Rajagopal for providing peptide samples and H. Winter for helpful discussions. Funding for this work was provided by the National Institutes of Health (No. 1 R01 EB003172-01 and No. 2 P20 016472-04) and the Procter and Gamble Company.

*Corresponding author.
furst@udel.edu

[1] Y. Tseng *et al.*, J. Biol. Chem. **277**, 18143 (2002).
[2] M. Gardel *et al.*, Phys. Rev. Lett. **91**, 158302 (2003).
[3] C. Y. Xu *et al.*, Biomacromolecules **6**, 1739 (2005).
[4] C. Veerman *et al.*, Macromolecules **39**, 6608 (2006).
[5] Y. Zimenkov *et al.*, J. Am. Chem. Soc. **128**, 6770 (2006).
[6] T. Savin and P. S. Doyle, Soft Matter **3**, 1194 (2007).
[7] D. Stauffer *et al.*, Adv. Polym. Sci. **44**, 103 (1982).
[8] J. F. Joanny, J. Phys. (France) **43**, 467 (1982).
[9] H. H. Winter and F. Chambon, J. Rheol. (N.Y.) **30**, 367 (1986); **31**, 683 (1987).
[10] J. C. Scanlan and H. W. Winter, Macromolecules **24**, 47 (1991).
[11] D. Adolf and J. E. Martin, Macromolecules **23**, 3700 (1990).
[12] D. Pochan *et al.*, J. Am. Chem. Soc. **125**, 11 802 (2003).
[13] B. Ozbas *et al.*, Phys. Rev. Lett. **93**, 268106 (2004).
[14] The peptide sequence is H_3N-VKVKVKVKV^{D}PPTKVTVKVKV-NH_2.
[15] J. C. Crocker and D. G. Grier, J. Colloid Interface Sci. **179**, 298 (1996).
[16] T. Savin and P. S. Doyle, Biophys. J. **88**, 623 (2005).
[17] T. G. Mason and D. A. Weitz, Phys. Rev. Lett. **74**, 1250 (1995).
[18] F. Gittes *et al.*, Phys. Rev. Lett. **79**, 3286 (1997).
[19] A. Palmer *et al.*, Rheol. Acta **37**, 97 (1998).
[20] J. Ferry, *Viscoelastic Properties of Polymers* (Wiley, New York, 1980).
[21] H. H. Winter and M. Mours, Adv. Polym. Sci. **134**, 165 (1997).
[22] J. E. Martin *et al.*, Phys. Rev. Lett. **61**, 2620 (1988).
[23] B. Derrida *et al.*, J. Phys. Lett. **44**, L701 (1983).